

Offline Correction of Atmospheric Effects on Single-Dish Radio Spectroscopy

TSUYOSHI SAWADA,^{1,2} CHIN-SHIN CHANG,¹ HAROLD FRANCKE,¹ LAURA GOMEZ,¹
JEFFREY G. MANGUM,³ YUSUKE MIYAMOTO,⁴ TAKESHI NAKAZATO,⁴ SUMINORI NISHIE,⁴
NEIL M. PHILLIPS,⁵ YOSHITO SHIMAJIRI,⁴ AND KANAKO SUGIMOTO⁴

¹*Joint ALMA Observatory, Alonso de Córdova 3107, Vitacura, Santiago 763-0355, Chile*

²*NAOJ Chile, National Astronomical Observatory of Japan, Alonso de Córdova 3788 Office 61B, Vitacura, Santiago 763-0492, Chile*

³*National Radio Astronomy Observatory, 520 Edgemont Road, Charlottesville, VA 22903, USA*

⁴*National Astronomical Observatory of Japan, 2-21-1 Osawa, Mitaka, Tokyo 181-8588, Japan*

⁵*European Southern Observatory, Karl-Schwarzschild-Strasse 2, Garching bei München 85748, Germany*

(Received 2020-11-12; Revised 2020-12-30; Accepted 2021-01-27)

Submitted to PASP

ABSTRACT

We present a method to mitigate the atmospheric effects (residual atmospheric lines) in single-dish radio spectroscopy caused by the elevation difference between the target and reference positions. The method is developed as a script using the Atmospheric Transmission at Microwaves (ATM) library built into the Common Astronomy Software Applications (CASA) package. We apply the method to the data taken with the Total Power Array of the Atacama Large Millimeter/submillimeter Array. The intensities of the residual atmospheric (mostly O₃) lines are suppressed by, typically, an order of magnitude for the tested cases. The parameters for the ATM model can be optimized to minimize the residual line and, for a specific O₃ line at 231.28 GHz, a seasonal dependence of a best-fitting model parameter is demonstrated. The method will be provided as a task within the CASA package in the near future. The atmospheric removal method we developed can be used by any radio/millimeter/submillimeter observatory to improve the quality of its spectroscopic measurements.

Keywords: Astronomy data reduction (1861) — Millimeter astronomy (1061) — Radio spectroscopy (1359) — Submillimeter astronomy (1647)

1. INTRODUCTION

The chopper-wheel method (e.g., Ulich & Haas 1976; Kutner & Ulich 1981) is commonly used for calibrating the amplitude of the data from single-dish radio telescopes,

$$T_A^* = \frac{P(\text{ON}) - P(\text{OFF})}{P(\text{OFF})} T_{\text{sys}} \quad , \quad (1)$$

where T_A^* is the antenna temperature corrected for the atmospheric attenuation and antenna losses, T_{sys} is the system noise temperature, $P(\text{ON})$ and $P(\text{OFF})$ are the detector readouts toward the target (ON) and astronomical-emission-free reference (OFF) positions, respectively (a detailed formulation is given in Section 2).

A fundamental assumption in Equation (1) is that the atmospheric emission/absorption is the same between the ON and OFF positions. When this assumption breaks-down, the subtraction of the sky emission in the ON and OFF measurements becomes imperfect and produces artifacts in the resultant calibrated data. A common cause of the non-optimal subtraction of the sky emission is the elevation difference between the ON and OFF positions. For isolated and compact targets like external galaxies, the difference can be minimized by acquiring the OFF position at the same elevation as the ON position. However such a mitigation is not possible for extended objects like the Galactic molecular clouds, which require carefully-chosen OFF positions, which are known to be free of source emission (i.e., CO in Galactic molecular clouds), at fixed celestial coordinates. In the case of the Atacama Large Millimeter/submillimeter Array (ALMA) Total Power Array (TP Array; [Iguchi et al. 2009](#)) observations of such objects, the separation between the ON and OFF positions can be as large as a few degrees.

As long as the atmospheric emission and absorption can be considered to be quasi-continuum within the instantaneous bandwidth of the spectrometer¹, the artifact is also quasi-continuum. It can be easily corrected, to the first order², by subtracting spectral baselines. However, that is no longer the case if relatively narrow lines from atmospheric species fall into the measured bandwidth. This issue is becoming more critical for mm and sub-mm observations due to the broad instantaneous bandwidths which modern instruments offer, given the existence of multiple telluric lines from species such as H₂O, O₂, and O₃ (Figure 1).

In this article, we present a method for offline (i.e., post-processing) correction of the atmospheric artifacts. The method itself is formulated in Section 2. We implemented the method within the Common Astronomy Software Applications package (CASA; [McMullin et al. 2007](#)) as described in Section 3. The verification of the method using the data from the ALMA TP Array is presented in Section 4.

2. METHOD

The detector (spectrometer) readouts toward the ON and OFF positions are, assuming the ideal single-sideband response³, written as

$$P(\text{ON}) = Gk \{ T_{\text{RX}} + \eta_l T_{\text{sky}}(\text{ON}) + \eta_l e^{-\tau(\text{ON})} T_{\text{CMB}} + (1 - \eta_l) T_{\text{amb}} + \eta_l e^{-\tau(\text{ON})} T_{\text{src}} \} \quad (2)$$

$$P(\text{OFF}) = Gk \{ T_{\text{RX}} + \eta_l T_{\text{sky}}(\text{OFF}) + \eta_l e^{-\tau(\text{OFF})} T_{\text{CMB}} + (1 - \eta_l) T_{\text{amb}} \} \quad (3)$$

where G is the system gain; k is the Boltzmann constant; T_{RX} is the receiver noise temperature; η_l is the feed efficiency ($1 - \eta_l$ corresponds to the rearward spillover, blockage, and ohmic losses; [Ulich & Haas 1976](#)); T_{sky} is the radiation temperature of the sky toward the line of sight; τ is the optical depth of the atmosphere toward the line of sight; T_{CMB} is the radiation temperature of the cosmic microwave background (CMB); T_{amb} is the ambient temperature; T_{src} is the radiation temperature

¹ In this article, we are concerned with spectral line observations only.

² To be more precise, the amplitude scaling also needs to be corrected, see Section 2, Equation (9).

³ The typical sideband rejection of the ALMA sideband-separating receivers (Bands 3–8) is 20 dB ([W. Dent, private communication](#)).

hence⁴

$$T_{\text{A}}^* \approx \{T_{\text{sky}}(\text{ON}) - T_{\text{sky}}(\text{OFF}) + (e^{-\tau(\text{ON})} - e^{-\tau(\text{OFF})}) T_{\text{CMB}} + e^{-\tau(\text{ON})} T_{\text{src}}\} e^{\tau(\text{OFF})} \quad (6)$$

while it should ideally be

$$T_{\text{A}}^* = T_{\text{src}} \quad . \quad (7)$$

Therefore, in order to mitigate the artifacts caused by the difference between the atmosphere toward the ON and OFF positions, the difference between Equations (6) and (7)

$$\begin{aligned} \Delta T_{\text{A}}^* &\approx \{T_{\text{sky}}(\text{ON}) - T_{\text{sky}}(\text{OFF}) + (e^{-\tau(\text{ON})} - e^{-\tau(\text{OFF})}) T_{\text{CMB}}\} e^{\tau(\text{OFF})} + (e^{\tau(\text{OFF}) - \tau(\text{ON})} - 1) T_{\text{src}} \\ &\equiv \Delta T_{\text{A}}^*(1) + \Delta T_{\text{A}}^*(2) \end{aligned} \quad (8)$$

needs to be computed using atmospheric models (e.g., the millimeter-wave propagation model [MPM] by [Liebe 1989](#); the atmospheric transmission at microwaves [ATM] by [Pardo et al. 2001](#)) and subtracted from the calibrated spectra. The first term corresponds to the residual atmospheric lines (plus quasi-continuum, which is eliminated by spectral baseline subtraction), while the second term indicates that T_{src} is incorrectly scaled by a factor of $\exp(\tau(\text{OFF}) - \tau(\text{ON}))$.

The second term $\Delta T_{\text{A}}^*(2)$ is not directly calculable, since T_{src} is unknown. Instead of subtracting $\Delta T_{\text{A}}^*(2)$ from T_{A}^* , the correction can be made by

$$\begin{aligned} T_{\text{A}}^*(\text{corrected}) &= \{T_{\text{A}}^* - \Delta T_{\text{A}}^*(1)\} e^{\tau(\text{ON}) - \tau(\text{OFF})} \\ &= T_{\text{src}} \quad . \end{aligned} \quad (9)$$

If we assume the atmospheric transmission of 95% at the quasi-continuum, 90% at the line (typical values for O₃ lines in ALMA Band 6 [211–275 GHz] observations; [Figure 1](#)), and the elevations of the ON and OFF positions of 50° and 49°, respectively, $\Delta T_{\text{A}}^*(1)$ amounts to $\simeq 0.2$ K after re-subtraction of a spectral baseline. On the other hand, $\Delta T_{\text{A}}^*(2)$ is about 0.1% and 0.2% of T_{src} , respectively, at the quasi-continuum and line frequencies. That is, $\Delta T_{\text{A}}^*(2)$ is smaller than $\Delta T_{\text{A}}^*(1)$, unless T_{src} is extremely high ($\gtrsim 100$ K) in that condition. It is also much smaller than the absolute flux accuracy ALMA currently offers, 5% in Bands 3 to 5 and 10% in Bands 6 to 8 ([Remijan et al. 2020](#)). Although $\Delta T_{\text{A}}^*(2)$ may become significant under some circumstances (in particular at low elevations), we have not been able to collect sufficient cases to validate it. Therefore, we focus on the correction expressed by $\Delta T_{\text{A}}^*(1)$ in this article and defer the validation of $\Delta T_{\text{A}}^*(2)$ to a future study.

3. IMPLEMENTATION

In order to verify the method, we wrote a script in CASA (version 5.6.1) which calculates the first term of the right-hand side of Equation (8)

$$\Delta T_{\text{A}}^*(1) \equiv \{T_{\text{sky}}(\text{ON}) - T_{\text{sky}}(\text{OFF}) + (e^{-\tau(\text{ON})} - e^{-\tau(\text{OFF})}) T_{\text{CMB}}\} e^{\tau(\text{OFF})} \quad (10)$$

and subtracts it from the calibrated spectra (T_{A}^*).

We use the ATM model ([Pardo et al. 2001](#)) to compute the radiation temperature and opacity of the atmosphere. The ATM library is integrated into CASA and accessible via its `atmosphere`

⁴ In ALMA TP Array observations, T_{sys} is measured at the OFF position. Although T_{sys} is not measured concurrently with OFF or ON measurements, the time-interpolated T_{sys} is used for calibration into individual T_{A}^* spectra. Therefore $T_{\text{sys}} \approx P(\text{OFF}) \exp(\tau(\text{OFF})) / (Gk\eta)$.

Toolkit functions. First, the altitude of the telescope and the atmospheric conditions (i.e., the temperature, pressure, and relative humidity at the ground level, and the precipitable water vapor [PWV]) are read from the metadata of the observations and passed to the `initAtmProfile` and `setUserWH2O` functions. Second, the spectral setup (i.e., the center frequency, channel spacing, and the total bandwidth of each spectral window) is also read from the metadata and used to invoke the `initSpectralWindow` function. Finally, the radiation temperature and opacity of the sky are obtained by the `getTrjSkySpec`, `getDryOpacitySpec`, and `getWetOpacitySpec` functions for every ON and OFF position, whose airmass (elevation) is read from the metadata and set to the `setAirMass` function.

The radiation temperature of the sky calculated by the `getTrjSkySpec` function, $T_{\text{sky}}^{\text{ATM}}$, already includes the CMB term (unless the CMB temperature is manually set to 0). That is,

$$T_{\text{sky}}^{\text{ATM}} = T_{\text{sky}} + e^{-\tau} T_{\text{CMB}} \quad (11)$$

and, therefore, Equation (10) can be rewritten into a simpler form

$$\Delta T_{\text{A}}^*(1) = \{T_{\text{sky}}^{\text{ATM}}(\text{ON}) - T_{\text{sky}}^{\text{ATM}}(\text{OFF})\} e^{\tau(\text{OFF})} \quad (12)$$

Additionally, the spectral response of the spectrometer is convolved with the $\Delta T_{\text{A}}^*(1)$ spectra if necessary.

Although some of the parameters for the `initAtmProfile` function are “fixed” as described above, the function also accepts some other “free” parameters, such as the atmosphere type (`atmType`, corresponding to the latitude and season), the altitude of the top of the modeled atmosphere (`maxAltitude`), the lapse rate (`dTem_dh`), and the scale height of water vapor (`h0`). The available parameters and their default values are summarized in Table 1. In the next section we explore what the best parameters are for ALMA TP Array data.

4. RESULTS AND DISCUSSION

We apply the method described above to a selection of archival data from the ALMA TP Array and present the results. The data are calibrated into T_{A}^* through the standard way (Equation 1; using CASA’s `sdcal` task) first, and then $\Delta T_{\text{A}}^*(1)$ (Equation 12) is subtracted.

4.1. Proof of Concept

Figure 2 shows an example in ALMA Band 3; the averaged T_{A}^* spectra before and after correction from seventeen execution blocks (EBs) for the scheduling block (SB) Thakeray_a.03_TP of the project 2015.1.00908.S. The OFF position was approximately at $-11'$ toward the R.A. direction from the field center. Therefore, during these measurements, the ON position was at lower and higher elevation than the OFF position before and after the transit, respectively. The spectra before correction demonstrate that the amplitude of the residual O_3 line at 110.84 GHz clearly correlates with the elevation difference between ON and OFF, as expected. The line is mostly eliminated in the spectra after the correction (i.e., subtracting $\Delta T_{\text{A}}^*(1)$). The ratios between the corrected and original T_{A}^* of the line are displayed in Figure 3. At the frequency resolution of these measurements (31 MHz), the line intensities are suppressed by more than an order of magnitude, excepting a few that are noise-dominated (small T_{A}^* without correction, i.e., observed around the transit).

Table 1. Parameters for the `initAtmProfile` function

Name	Explanation	Default value
<code>altitude</code>	Site altitude	5000 m ^a
<code>temperature</code>	Ambient temperature	270 K ^a
<code>pressure</code>	Ambient pressure	560 hPa ^a
<code>maxAltitude</code>	Altitude of the top of the modelled atmosphere	48 km ^b
<code>humidity</code>	Humidity	20 % ^a
<code>dTem_dh</code>	Derivative of temperature with respect to height	-5.6 K km ⁻¹
<code>dP</code>	Initial pressure step	10 hPa
<code>dPm</code>	Pressure multiplicative factor for steps	1.2
<code>h0</code>	Scale height for water	2 km
<code>atmType</code>	Atmospheric type	1 ^c
<code>layerBoundaries</code>	Altitude of user-defined temperature profile	—
<code>layerTemperature</code>	User-defined temperature profile	—

^aWe use the values read from the metadata (see Section 3).

^bWe use 120 km instead of the default value in this article, unless otherwise noted (see Section 4.2).

^cEnumerated to 1 (*tropical*), 2 (*mid latitude summer*), 3 (*mid latitude winter*), 4 (*sub-arctic summer*), and 5 (*subarctic winter*).

As mentioned in Section 1, the elevation difference between the ON and OFF positions can be minimized by using OFF positions that are at the same elevation as their respective ON positions for isolated and compact objects. However, in practice, it is not always possible to keep the elevations of the ON and OFF positions exactly the same, due to, e.g., the diurnal motion and the strategy of mapping observations. Therefore the correction is also worth applying for such cases. Figure 4 shows the profile map of the 231.28 GHz O₃ line in ALMA Band 6 before and after correction. During the measurement which employed the On-The-Fly mapping technique (Mangum et al. 2007; Sawada et al. 2008), the OFF position was taken at constant elevation +10' toward the azimuthal direction from the field center, rather than the individual ON positions. The spatial gradient of the residual O₃ line along the elevation axis (at the position angle of -103° with respect to the equatorial coordinates) seen in the uncorrected (original) data is mostly eliminated from the corrected data.

4.2. Parameter Selection

A few more O₃ line profiles at higher spectral resolutions are presented in Figure 5: 154.05 GHz in Band 4, 231.28 GHz in Band 6, 355.02 GHz in Band 7, and 481.62 GHz in Band 8. Three `atmType` values, out of the five available options⁵, are attempted to correct the residual lines. The `atmType` parameter controls the vertical profiles of the temperature and pressure of upper atmosphere and the distribution of the molecular species. Although none of the models can completely eliminate the

⁵ The other two are for subarctic regions and therefore should be unsuited for the data from ALMA TP Array, located at latitude 23° S.

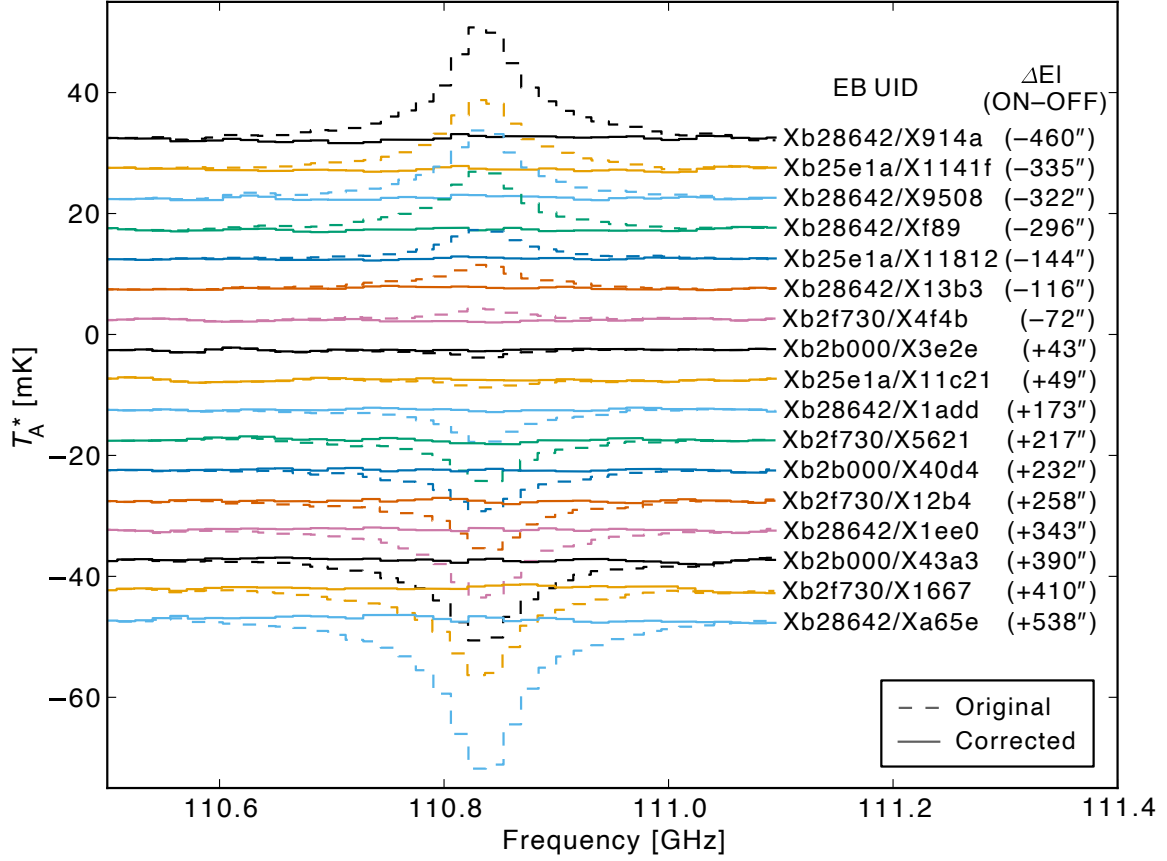


Figure 2. The averaged T_A^* spectra (+offsets) of the 110.84 GHz O_3 line from 17 EBs for the SB Thakray_a_03_TP. The observations were made in 2016 May. The dashed and solid lines are the spectra before and after correction, respectively. The spectra are sorted by the hour angles of the observations. The unique IDs (UIDs) of the EBs are annotated on the right (the common prefix, “uid://A002/”, is omitted), along with the median elevation differences between the ON (map center) and OFF positions in the parentheses. The *mid latitude summer* model (`atmType = 2`) is used for the correction.

line, the *tropical* model (`atmType = 1`) tends to produce the best results in these cases, and the *mid latitude summer* model (`atmType = 2`) is slightly worse. The best model may, however, be dependent on the observing seasons, as discussed in Section 4.3, as well as the species and transitions. The peak line intensities are suppressed by factors of ≈ 10 –20, if the best models are used, for the 154.05, 231.28, and 355.02 GHz lines. For the 481.62 GHz line, the suppression of the peak intensity is about a factor of 4.

The `maxAltitude` of 120 km was used to calculate the corrected spectra in Figure 5. In addition, for the 231.28 GHz line (panel b), the corrected spectrum using `maxAltitude = 48` km, which is the default value of the `initAtmProfile` function, is also drawn. It demonstrates that the 48 km `maxAltitude` is not sufficient, leaving a sharp residual at the center frequency of the line. Figure 6 shows the computed number densities of the H_2O , O_3 , CO, and N_2O molecules and their cumulative fraction as a function of altitude. A few % of the O_3 molecules are distributed above 48 km. Although being a small fraction compared with the bulk at lower altitude, it results in a remarkably deficient correction of the line due to the reduced pressure broadening, as shown above. Therefore `maxAltitude = 120` km is used in this article, unless otherwise noted.

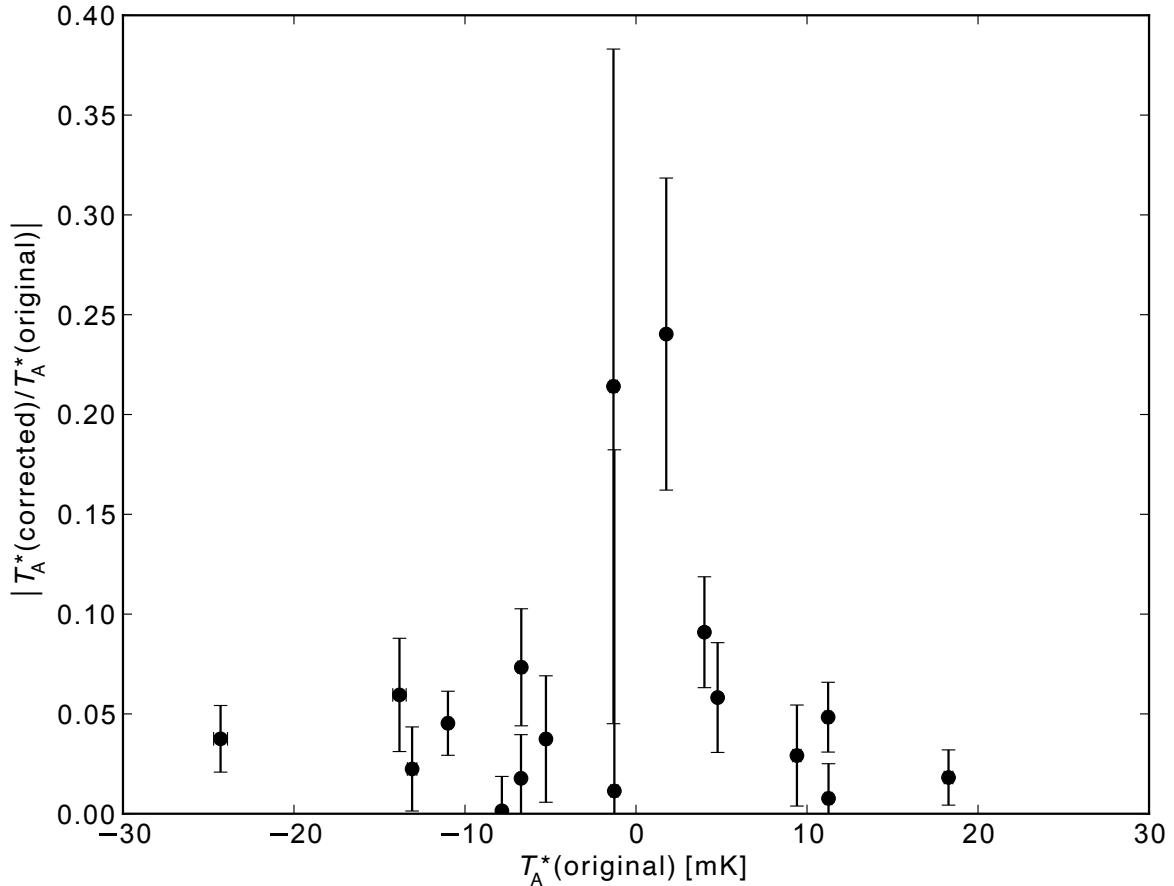


Figure 3. The ratios between the corrected and original T_A^* , at the center frequency of the line, for the spectra shown in Figure 2. The error bars indicate the 1σ noise.

The residual line features after correction may be due to discrepancies between the ATM models and the actual atmospheric profiles. We evaluate the discrepancy by comparing the ATM model for uid://A002/Xb020f7/X45ad (Figure 5b) with meteorological reanalysis datasets from the second Modern-Era Retrospective analysis for Research and Applications (MERRA-2; Gelaro et al. 2017). Figure 7 shows the vertical profiles of the pressure (p), temperature, and the column densities of O_3 and H_2O molecules. The `atmType` = 1 profiles of temperature and O_3 column density are closest among the three models to those from MERRA-2. This appears to be consistent with the fact that the correction works best with `atmType` = 1. The O_3 profiles, though, reveal a few differences between the MERRA-2 data and the ATM models:

1. Excess O_3 abundance is seen in the MERRA-2 data at the mesosphere ($p \lesssim 0.3$ hPa) compared with the ATM models. This is attributed to the diurnal variation of mesospheric ozone abundance (e.g., Vaughan 1982; Pardo et al. 1998); the excess disappears in the daytime MERRA-2 data, although not shown here.
2. The O_3 abundance in the ATM models at the lower mesosphere and upper stratosphere (≈ 0.3 –5 hPa) is slightly less than that in the MERRA-2 data.
3. At the middle of the stratosphere (≈ 10 –30 hPa), the ATM model (`atmType` = 3, in particular) provides less O_3 than MERRA-2.

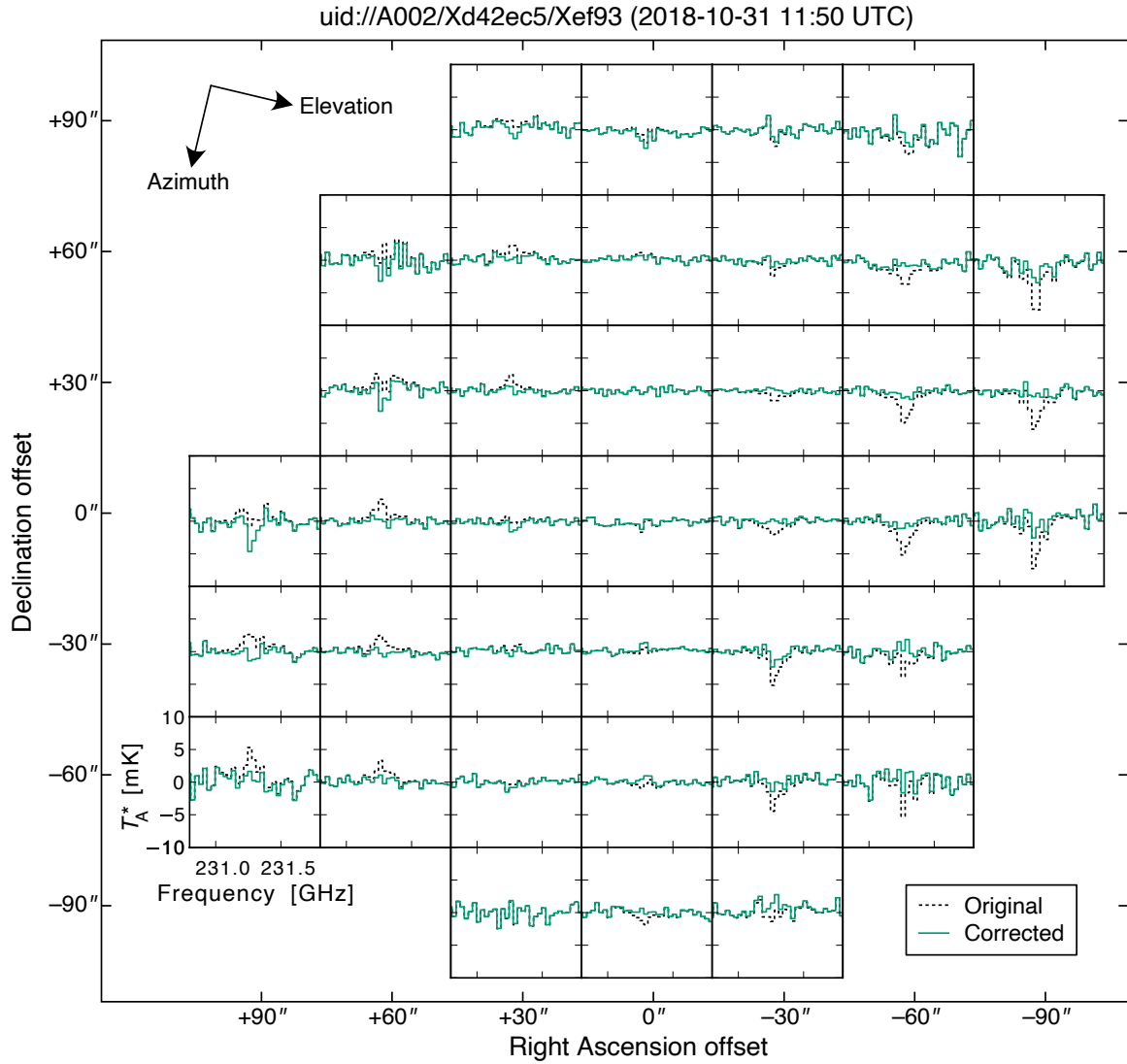


Figure 4. The 231.28 GHz O_3 line profile map made from the EB UID uid://A002/Xd42ec5/Xef93 (SB NGC4038_a.06_TP, project 2018.1.00272.S). Each panel represents a $30'' \times 30''$ area. The dashed and solid lines are the spectra before and after correction (with the *mid latitude summer* model), respectively. The equatorial coordinates are shown as offsets with respect to $(\text{R.A.}, \text{Decl.})_{\text{J2000}} = (12^{\text{h}}01^{\text{m}}53^{\text{s}}.1, -18^{\circ}52'32'')$. The directions of the horizontal axes (azimuth–elevation) at the time of the execution are drawn at top left. The data have been smoothed and resampled to 31 MHz resolution/spacing to improve the signal-to-noise ratio.

4. The O_3 abundance in the ATM models is largely discrepant with the MERRA-2 data at the lower stratosphere and troposphere ($\gtrsim 50$ hPa). However, due to the large pressure broadening compared with the instantaneous bandwidth, the impact of this component on the application of the method to ALMA TP Array data is not significant (i.e., mostly eliminated by spectral baseline subtraction).

It is expected that the correction may improve if the realistic atmospheric profiles from MERRA-2 can be used. However we cannot quantitatively prove this expectation, because CASA’s `atmosphere` tool does not provide the interface to directly control the profiles (except for the temperature, cf.

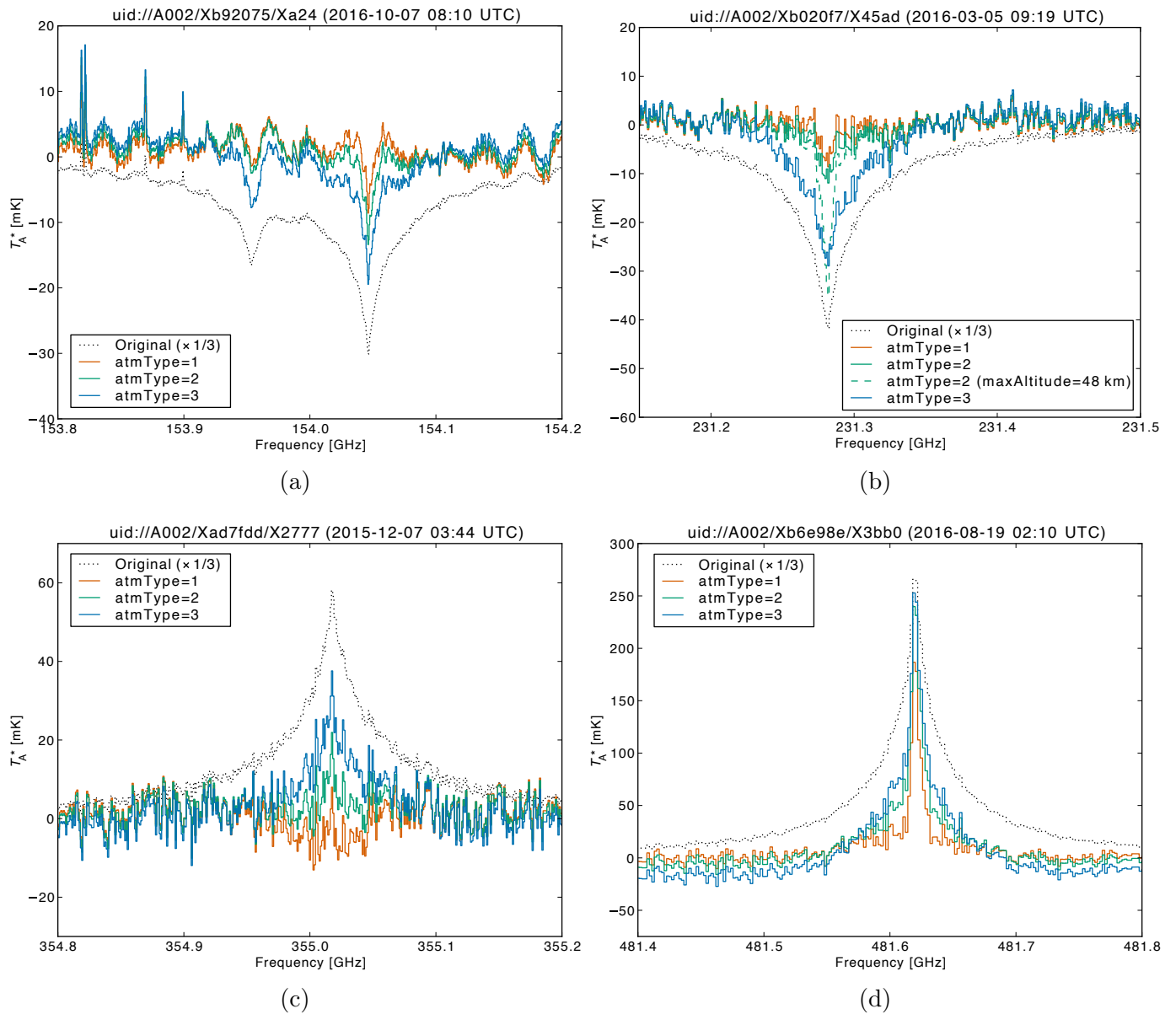


Figure 5. The uncorrected and corrected spectra of the O_3 lines in (a) ALMA Band 4 (EB uid://A002/Xb92075/Xa24, SB L1527_a.04_TP, project 2016.1.01541.S), (b) Band 6 (EB uid://A002/Xb020f7/X45ad, SB M83_a.06_TP, project 2015.1.00121.S), (c) Band 7 (EB uid://A002/Xad7fdd/X2777, SB NGC253_a.07_TP, project 2015.1.00274.S), and (d) Band 8 (EB uid://A002/Xb6e98e/X3bb0, SB NGC_6240_a.08_TP, project 2015.1.00717.S). The date/time shown at the top of each panel is the centroid of the on-source integrations. The uncorrected spectra (dotted lines) are divided by 3 so that they fit into the axes scale. The corrected spectra using three atmType values with maxAltitude = 120 [km] are drawn as solid lines; atmType = 1 (*tropical*), 2 (*mid latitude summer*), and 3 (*mid latitude winter*). For the Band 6 data (top right), the corrected spectrum using atmType = 2, maxAltitude = 48 [km] is also drawn as dashed line.

Table 1). Instead, we correlate the discrepancies described above with the residual line features in a semi-quantitative way.

We estimate the $\Delta T_A^*(1)$ (hereafter referred to as ΔT_A^* for simplicity) component for a layer of the atmosphere within a certain range of pressure (altitude) by taking the difference of ΔT_A^* spectra calculated using two values of `maxAltitude`. Figure 8a–c show the ΔT_A^* components corresponding to six layers ($p < 0.3$, 0.3–1, 1–3, 3–10, 10–30, and 30–100 hPa) along with the corrected spectra with `atmType` = 1, 2, and 3 (same as those shown in Figure 5b), respectively, for EB uid://A002/Xb020f7/X45ad. Figure 8d shows the ratio (hereafter R_{NT}), between the ATM model and MERRA-2 data, of the product of the O₃ column density (Figure 7c) and temperature (Figure 7b). Since the 231.28 GHz O₃ line is optically thin (cf. Figure 1, unless the airmass is very high), the product of the column density and temperature is roughly proportional to the observed atmospheric line emission originating in the corresponding altitude.

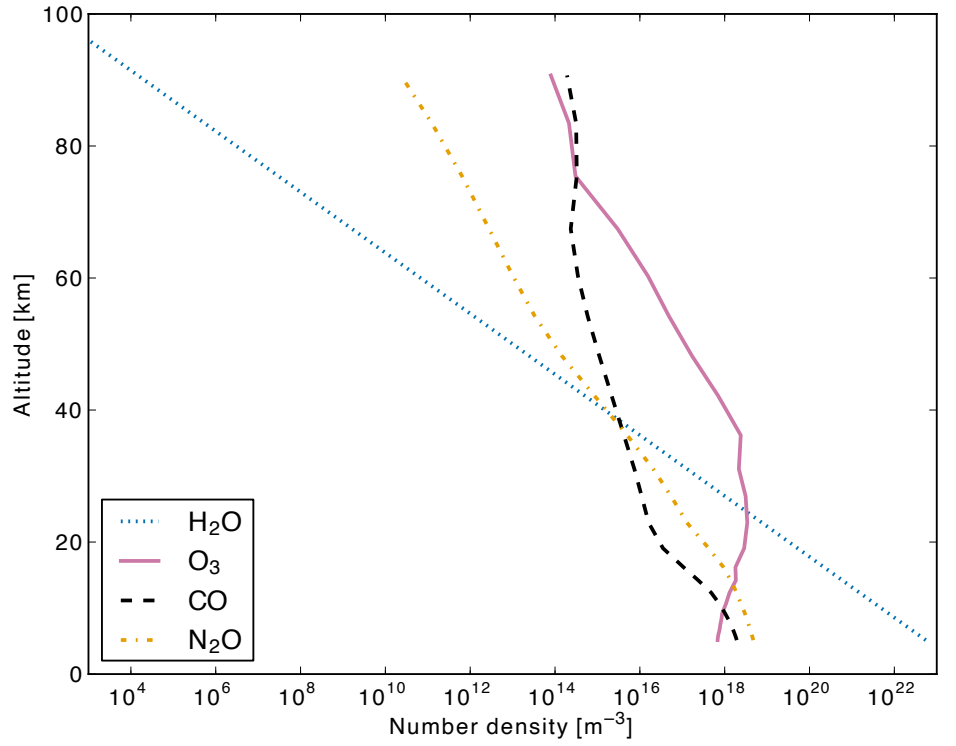
Now we revisit the discrepancies between the MERRA-2 data and the ATM model described above:

1. Under-abundance of O₃ in the ATM models at $p \lesssim 0.3$ hPa. The R_{NT} is ≈ 0.5 at 0.3 hPa and gets lower at higher altitude. Therefore the corresponding ΔT_A^* component is under-corrected by a factor of two or more. However, since the amplitude of this component is not very high (comparable to the noise level), its impact on the correction is likely not significant for this particular dataset.
2. Under-abundance at ≈ 0.3 –5 hPa. The corresponding ΔT_A^* component is estimated, as the sum of the 0.3–1 and 1–3 hPa spectra in Figure 8, to have the peak intensity of $\simeq 40$ mK and the full width at half maximum (FWHM) of $\simeq 10$ MHz. Since R_{NT} is typically 0.7–0.8, this component is under-corrected by a few $\times 10\%$, i.e., $\simeq 10$ mK. This seems to largely explain the residual feature around the line center, albeit possible over-correction.
3. Under-abundance (in particular `atmType` = 3) at ≈ 10 –30 hPa. The corresponding ΔT_A^* component has $\simeq 20$ mK peak intensity and $\simeq 100$ MHz FWHM. The R_{NT} varies with altitude and ranges between $\simeq 0.4$ –1. As a rough estimate, we assume the typical ratio to be 0.7, i.e., the component is under-corrected by about 40% $\simeq 8$ mK. It, along with the under-abundance at higher altitude (typically $R_{NT} \simeq 0.7$), is likely responsible to the residual feature with wings.

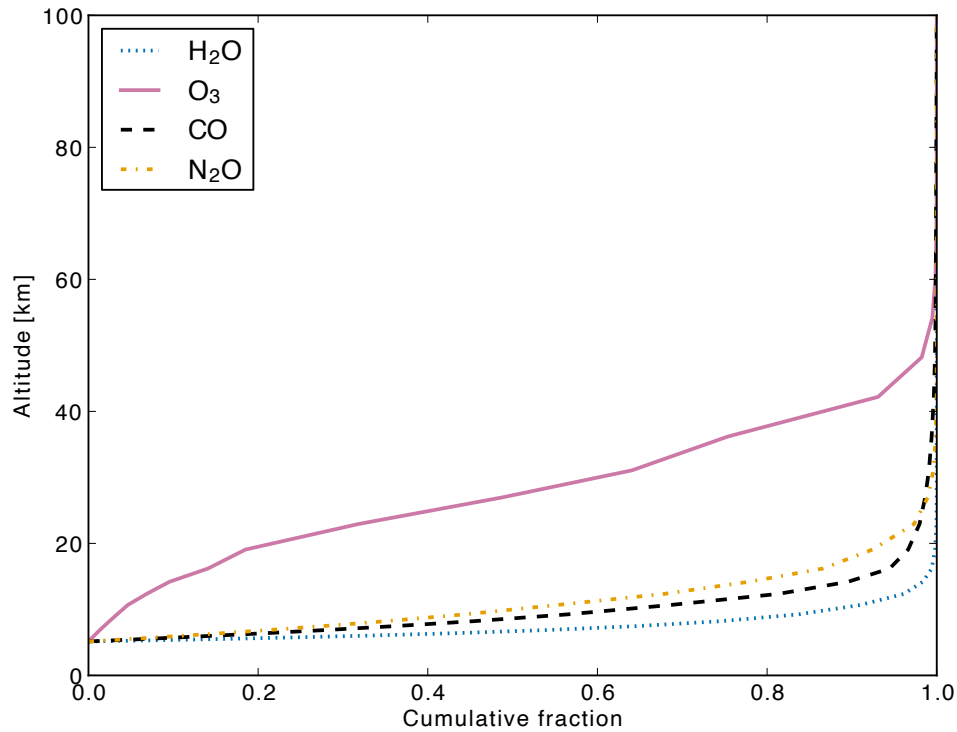
We showed that the correction may become better if the atmospheric model is improved. However, such an improvement is not available in the short term. Therefore, in the following subsection, we seek best-fitting parameters for the current model.

4.3. Seasonal and Daily Variations

For the datasets shown in Figure 5, the *tropical* model (`atmType` = 1) seems to work the best. However, the best parameter(s) may vary from season to season, and/or between day and night. In order to see if such a variation exists, we analyze the 231.28 GHz O₃ line in the sixteen datasets listed in Table 2. The line is chosen because it has often been observed simultaneously with the CO $J = 2$ –1 line at 230.54 GHz. The datasets are arbitrarily picked from the public data in the archive, spreading through the seasons, daytime (between midday and sunset) and nighttime (between midnight and sunrise). In addition to `atmType`, we also change secondary parameters, namely the lapse rate (`dTem_dh`) and water scale height (`h0`). The parameter set (`dTem_dh` [K km⁻¹], `h0` [km]) = (−6.8, 1.5)



(a)



(b)

Figure 6. (a) The number densities and (b) cumulative column density fractions of the H_2O , O_3 , CO , and N_2O molecules as a function of altitude above sea level. Computed by CASA/ATM using the *mid latitude summer* (`atmType = 2`) model for the atmospheric conditions of 268 K ambient temperature, 556 hPa pressure, 50% humidity, and 1.4 mm PWV (close to the conditions for `uid://A002/Xb020f7/X45ad`, Figure 5b).

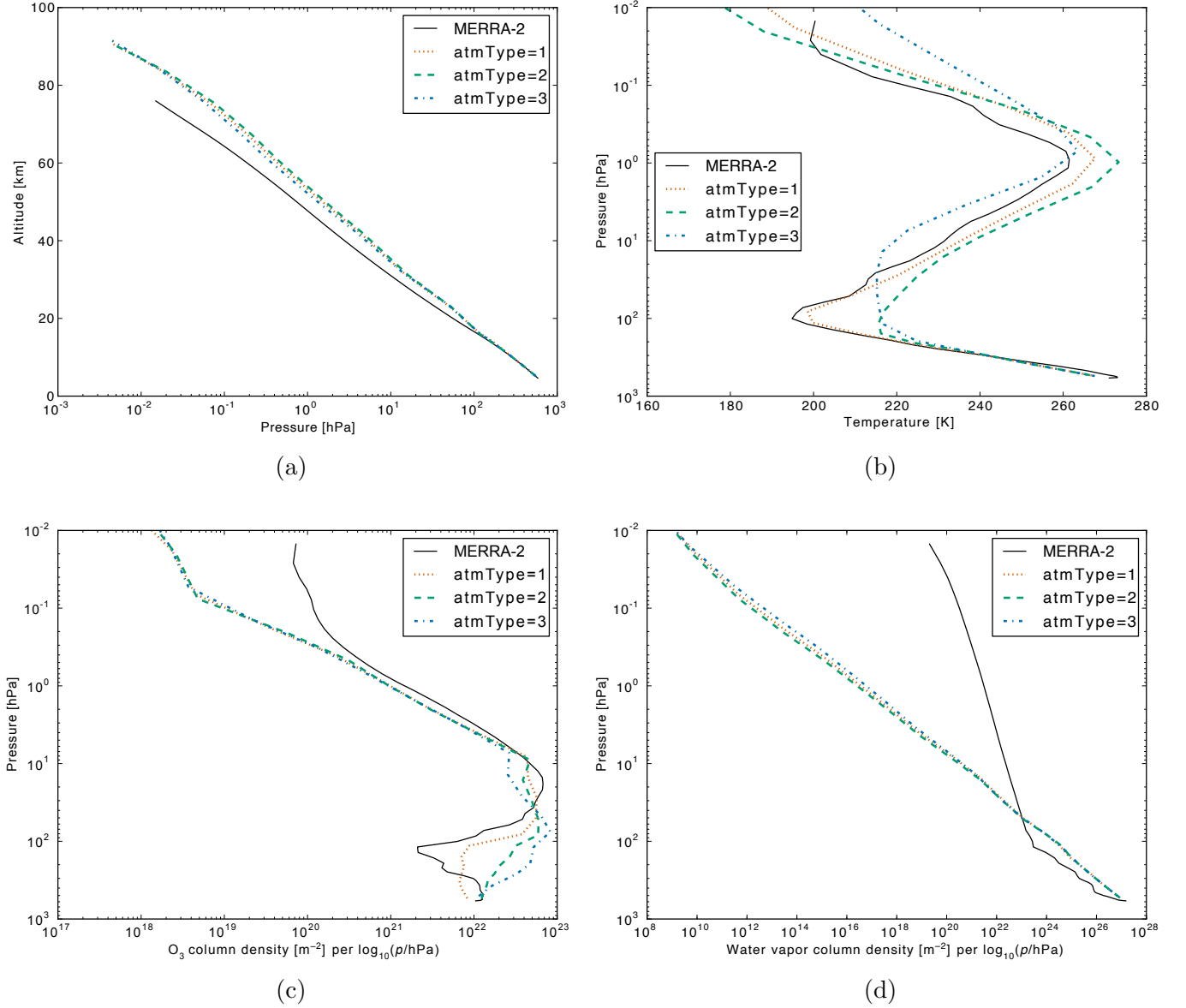


Figure 7. (a) The pressure p as a function of altitude for uid://A002/Xb020f7/X45ad. The three-hourly instantaneous datasets from MERRA-2 (Global Modeling and Assimilation Office (GMAO) 2015a,b) at the closest spatial and temporal grids to those of the ALMA dataset, namely ($67^{\circ}5$ W, $23^{\circ}0$ S) and 2016-03-05 09:00 UTC, respectively, are compared with the ATM models with `atmType` = 1 (*tropical*), 2 (*mid latitude summer*), and 3 (*mid latitude winter*). (b) The vertical profile of the temperature. (c) The vertical profile of the O_3 column density per unit $\log_{10}(p/\text{hPa})$. (d) Same as (c), but for water vapor.

estimated by Stirling et al. (2004), as well as the function’s default $(-5.6, 2.0)$, is attempted. Upon the comparison, the data are smoothed/resampled to the common resolution/spacing of 2 MHz.

The spectra for the representative seven datasets (observed around the solstices and equinoxes, daytime and nighttime) are shown in Figure 9. For the data taken in summer (the second row), the residual line is minimized by using the *tropical* model (`atmType` = 1). For those taken in winter (the fourth row), on the other hand, the *mid latitude summer* model (`atmType` = 2) works better, the

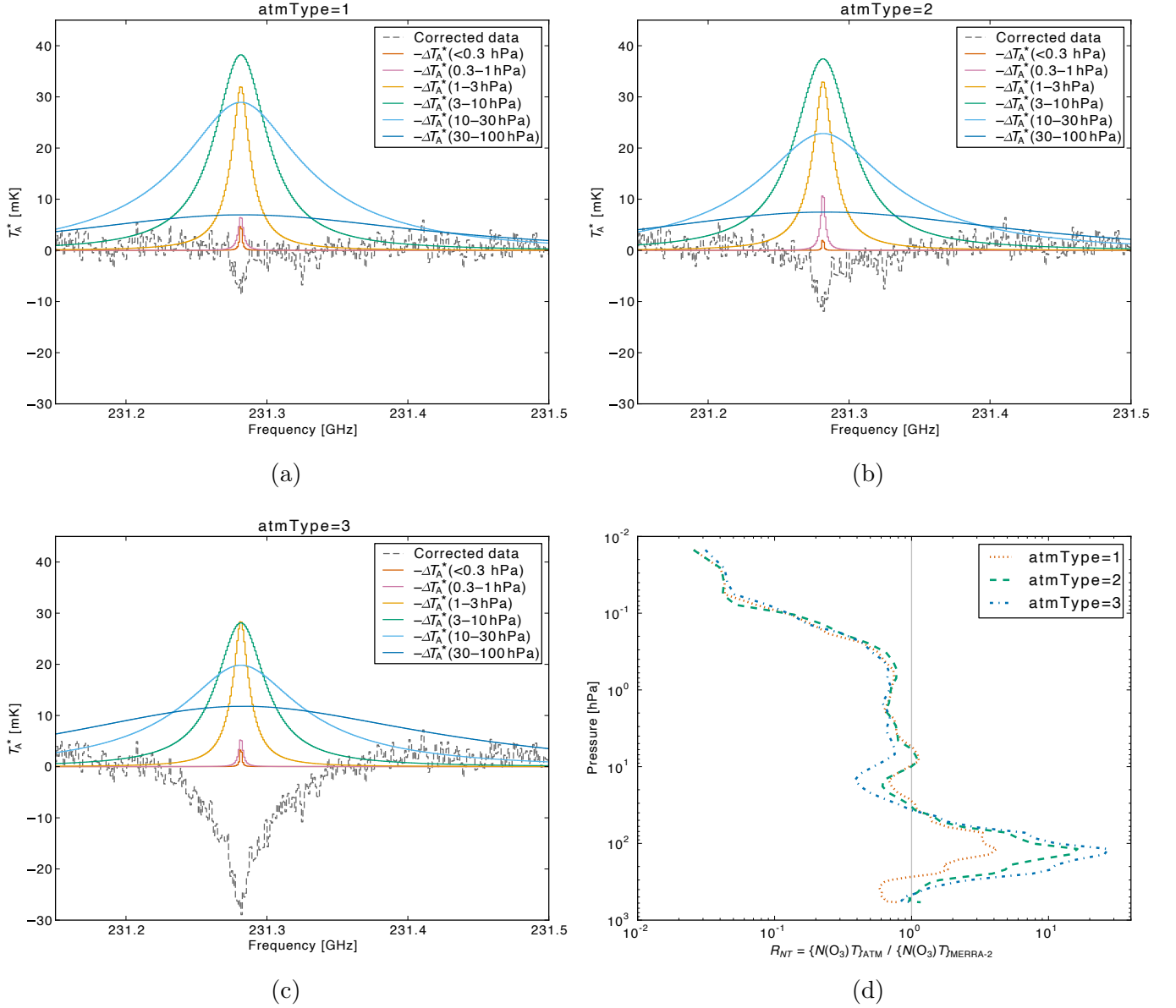


Figure 8. (a), (b), (c) The ΔT_A^* components corresponding to six layers of the atmosphere ($p < 0.3$, 0.3–1, 1–3, 3–10, 10–30, and 30–100 hPa) and the corrected spectra using $\text{atmType} = 1, 2,$ and 3 , respectively, for uid://A002/Xb020f7/X45ad. The signs of the ΔT_A^* spectra are flipped for visibility. Note that the quasi-continuum component is already removed by spectral baseline subtraction, which is done at $\simeq 500$ MHz from the line center. (d) The ATM-to-MERRA-2 ratio of the product of the O_3 column density and temperature, R_{NT} .

tropical model over-correcting the inner line wings. Varying the parameter set (`dTem_dh`, `h0`) causes much smaller difference than varying `atmType` does and it is hard to tell which one is better.

The results from the sixteen datasets are shown in Figure 10; the ratio between the maximum line intensities of the corrected and original spectra is plotted as a function of observing season, for the daytime and nighttime observations. These comparisons indicate that, as already demonstrated for the representative seven datasets, the *tropical* ($\text{atmType} = 1$) and *mid latitude summer* (2) models

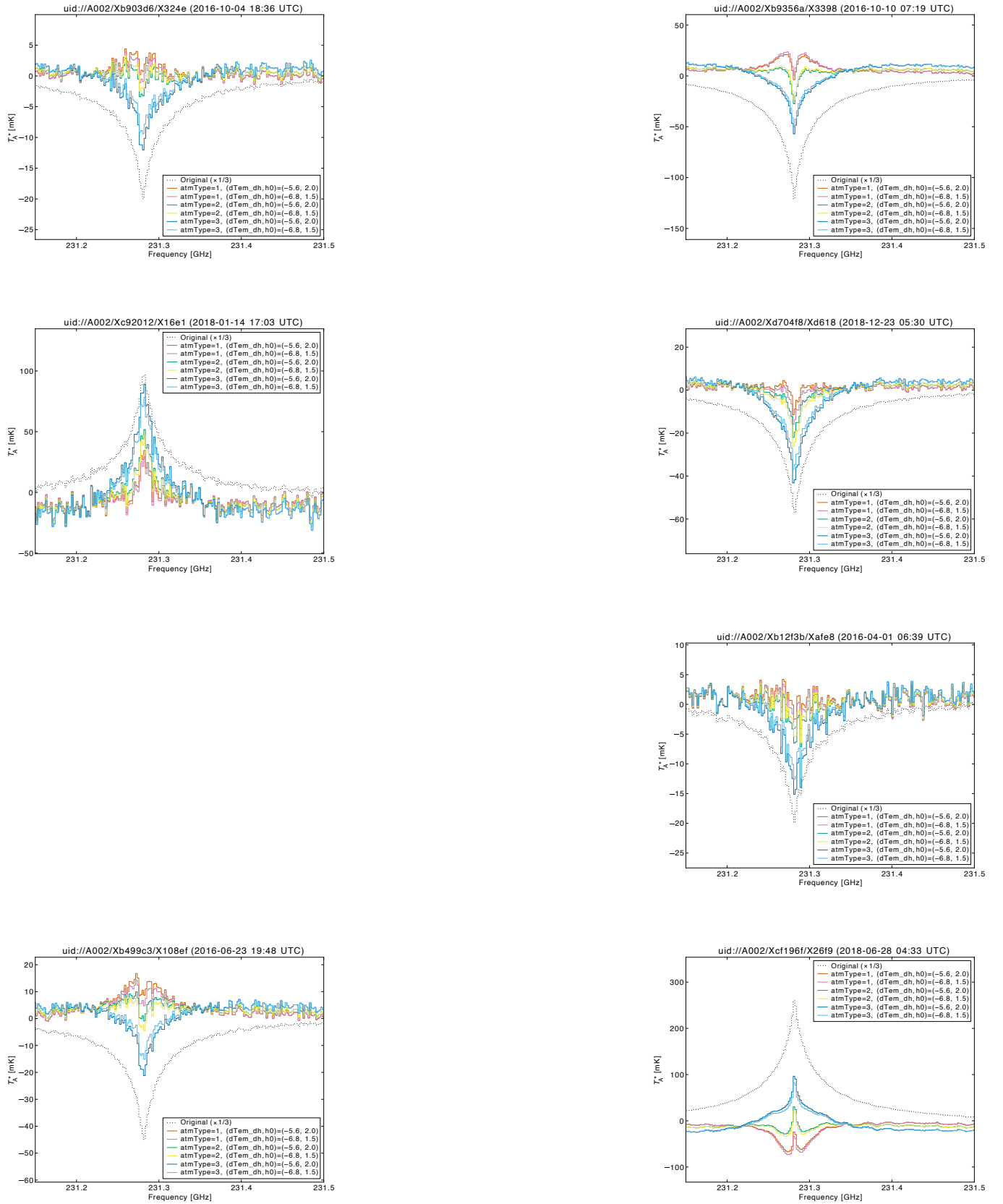


Figure 9. The uncorrected and corrected spectra of the 231.28 GHz O_3 line from the seven EBs. The EB UID and observing date/time are shown at the top of each panel. The panels are sorted by the season (spring, summer, autumn, and winter from top to bottom), and those on the left and right sides are for the data observed in the daytime and nighttime, respectively. The uncorrected spectra (dotted lines) are divided by 3 so that they fit into the axes scale.

Table 2. The properties of the EBs used to study the seasonal/daily variation

EB UID ^a	Project code	SB name ^b	Date and time ^c UTC	PWV (mm)	Temperature (K)	Pressure (hPa)	Humidity (%)	In Fig. 9
Xc92012/X16e1 ^d	2016.1.01346.S	AGAL010..a	2018-01-14 17:03	1.63	275.4	554.9	37	Yes
Xb046c2/X406f	2015.1.00121.S	M83_a	2016-03-09 05:05	1.27	268.4	556.6	60	No
Xb12f3b/Xafe8	2015.1.00121.S	M83_b	2016-04-01 06:39	1.43	272.9	558.3	11	Yes
Xc04da7/X7f4	2015.1.00121.S	M83_a	2017-05-14 05:12	1.07	264.7	556.6	51	No
Xb499c3/X108ef	2015.1.00357.S	G286_5_a	2016-06-23 19:48	0.85	272.1	554.8	10	Yes
Xcf196f/X26f9	2017.1.00716.S	G333.01_a	2018-06-28 04:33	0.72	263.6	553.6	56	Yes
Xb54d65/X37e0	2015.1.01539.S	G28.23_a	2016-07-13 06:54	0.54	261.7	553.3	16	No
Xb57bb5/X2839	2015.1.00357.S	G286_5_a	2016-07-17 18:07	0.52	270.4	554.9	3	No
Xb638bc/X1df2	2015.1.00667.S	AG22.36+_l	2016-08-03 05:02	0.72	264.6	556.5	14	No
Xb66ea7/X599c	2015.1.00357.S	G286_5_a	2016-08-09 17:33	0.31	270.3	554.1	4	No
Xd1daeb/X42d0	2017.1.00093.S	YSO45_a	2018-09-11 05:54	0.64	267.6	555.5	13	No
Xb9356a/X3398	2016.1.00203.S	LMC_N166_a	2016-10-10 07:19	0.68	264.2	553.8	36	Yes
Xb903d6/X324e	2016.1.00386.S	M83_c	2016-10-04 18:36	0.70	273.1	554.9	5	Yes
Xba1cd8/X41d4	2016.1.00386.S	M83_a	2016-11-03 16:20	0.65	277.3	556.7	1	No
Xd704f8/X74a5 ^d	2018.1.00443.S	G343.756_a	2018-12-22 15:40	2.04	275.0	556.0	27	No
Xd704f8/Xd618	2018.1.00770.S	Hummingb_a	2018-12-23 05:30	0.61	269.4	555.7	26	Yes

^aThe common prefix, “uid://A002/”, is omitted.

^bThe common suffix, “_06_TP”, is omitted.

^cThe centroid of the on-source integrations. The Chilean standard time and summer time are $-4:00$ and $-3:00$, respectively, from UTC.

^dMultiple targets were observed in the EB. Only the first one is used for the analysis.

work best for the data taken in summer and winter, respectively, at least for this particular line. The maximum line intensities are suppressed by factors of ≈ 10 – 20 , if the appropriate parameters are chosen. The difference between the daytime and nighttime observations is not clear. Although the diurnal variation of mesospheric O_3 abundance is known to exist, the amplitude of the emission from that altitude is low (Section 4.2).

4.4. Molecules Other Than Ozone

The narrow lines that show up in the mm to sub-mm regime (Figure 1) are mostly from O_3 molecules. The line profiles of other molecules that are abundant in the lower atmosphere (e.g., H_2O and O_2) are highly pressure-broadened and hence outside the scope of the analyses in this section (i.e., the lines are much broader than the ALMA’s instantaneous bandwidth, 2 GHz per baseband).

Figure 11 shows an exceptional case; the 233.95 GHz line of the oxygen isotopologue $^{16}O^{18}O$ before and after the correction. Due to the species’ rarity, the narrow peak of the line originating from the upper atmosphere is visible (cf. Pardo et al. 1995). The correction is not as good as that for the O_3

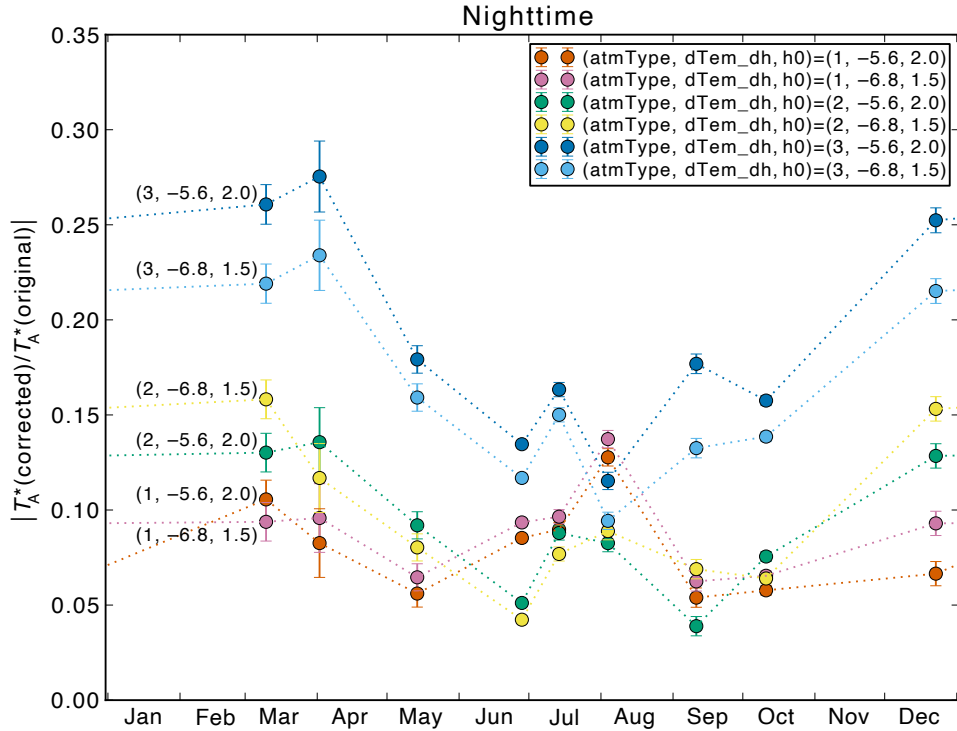
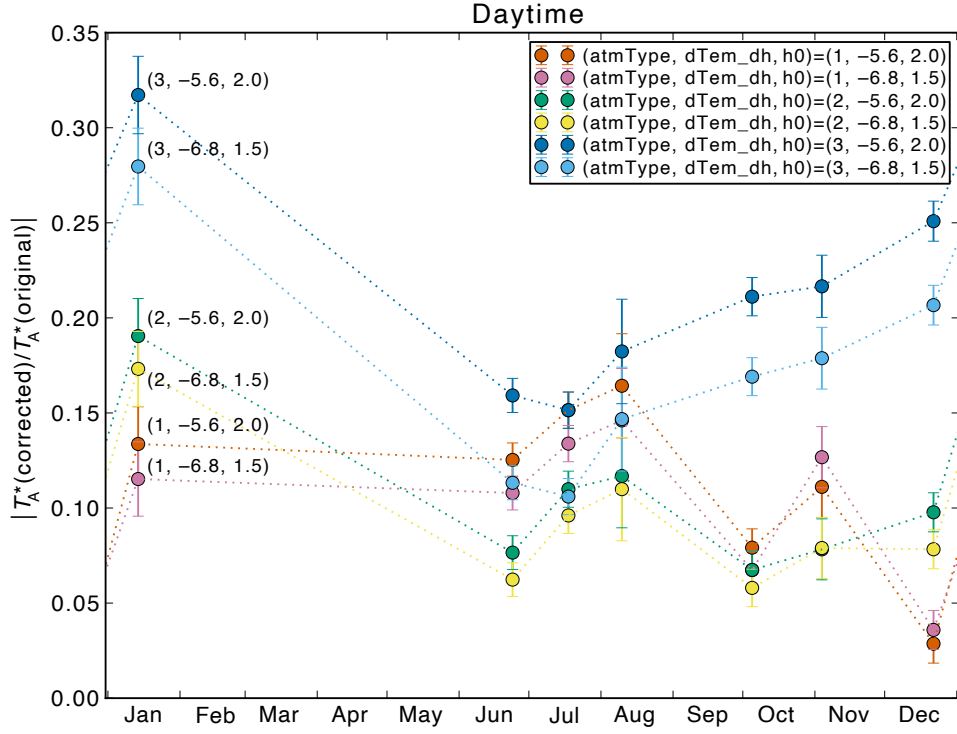


Figure 10. The ratios between the maximum intensities of the corrected and original 231.28 GHz O_3 line spectra for the datasets listed in Table 2, as a function of observing date. (a) The datasets observed in the daytime, (b) those in the nighttime. The error bars indicate the 1σ noise. Note that the maximum intensities in the corrected spectra do not necessarily appear at the center of the line (see Figure 9).

lines presented earlier; all the three `atmType` values similarly result in over-correcting the line, with a sharp feature at the line center.

The poor correction can be, at least partially, attributed to the difference between the vertical atmospheric profiles from ATM and MERRA-2. The emission from a given altitude is proportional to the product of the number density of the molecule and temperature as mentioned in Section 4.2 and, in the case of oxygen (which is supposed to be well-mixed in the atmosphere), it is also proportional to the pressure (assuming the ideal gas law). Figure 12 shows the pressure ratio between ATM and MERRA-2 as a function of altitude. The typical ratios at the altitudes of 20–35, 35–60, and > 60 km are $\simeq 1.5$, 2, and 3, respectively, with `atmType` = 1. That is, the correction ΔT_A^* is likely overestimated by these factors at these altitude ranges. Therefore we determine the ΔT_A^* components for 20–35, 35–60, and > 60 km altitudes as we did in Section 4.2, and divide them by 1.5, 2, and 3, respectively.

The result is shown in Figure 11 as a dashed line. Although the correction is still not very accurate near the center of the line (nevertheless, the peak intensity is suppressed by about a factor of 4 relative to its uncorrected intensity), the line wing is much better corrected. Empirically, the residual can be mostly eliminated by further subtracting the pressure-corrected ΔT_A^* for the altitude range of 35–60 km (in other words, if the pressure correction by a factor of 2 was not applied), as shown in Figure 11 as a dash-dotted line. Although a naive interpretation of this calculation may lead to an incorrect estimate of the abundance by a factor of 2, this interpretation seems unlikely because oxygen is expected to be well-mixed in the atmosphere. We leave the root cause of the less-than-optimal modeling unknown; it is beyond the scope of this article to completely diagnose the limitations of the built-in ATM atmosphere models and comparison with MERRA-2.

4.5. Caveats

We have analyzed the seasonal/daily variation of the 231.28 GHz O₃ line in Section 4.3 and demonstrated that the *tropical* and *mid latitude summer* models work the best for the data taken in summer and winter, respectively. This might possibly be explained qualitatively as follows; the atmosphere at the ALMA site (located near the tropic of Capricorn, the zenith angle of the sun at the transit ranging from 90° in summer to 44° in winter) is tropical-like in summer and mid-latitude-like in winter. However, this could also be a coincidence. In fact, the 481.62 GHz O₃ line data shown in Figure 5d is contradictory, the *tropical* model being the best while the dataset was taken in August (winter). Therefore a future study using a larger set of data is required. Such a study might also contribute to improving the atmospheric model.

In our implementation, the differences of the T_{sky} and τ between the ON and OFF positions are assumed to solely depend on elevation, i.e., a stable and isotropic atmosphere is assumed. In reality temporal and directional variation of the atmosphere causes additional artifacts. In the case of ALMA TP Array, theoretically, the short-timescale variation of (the wet component of) the atmosphere can be traced to some extent by using the data from the water vapor radiometer (Nikolic et al. 2013), which is equipped on each antenna and records the 183 GHz water line emission at an interval of ≈ 1 s. However, the possibility of improving the correction by taking the short-timescale variation into account has not been explored and will be a topic of a future study.

5. CONCLUSIONS

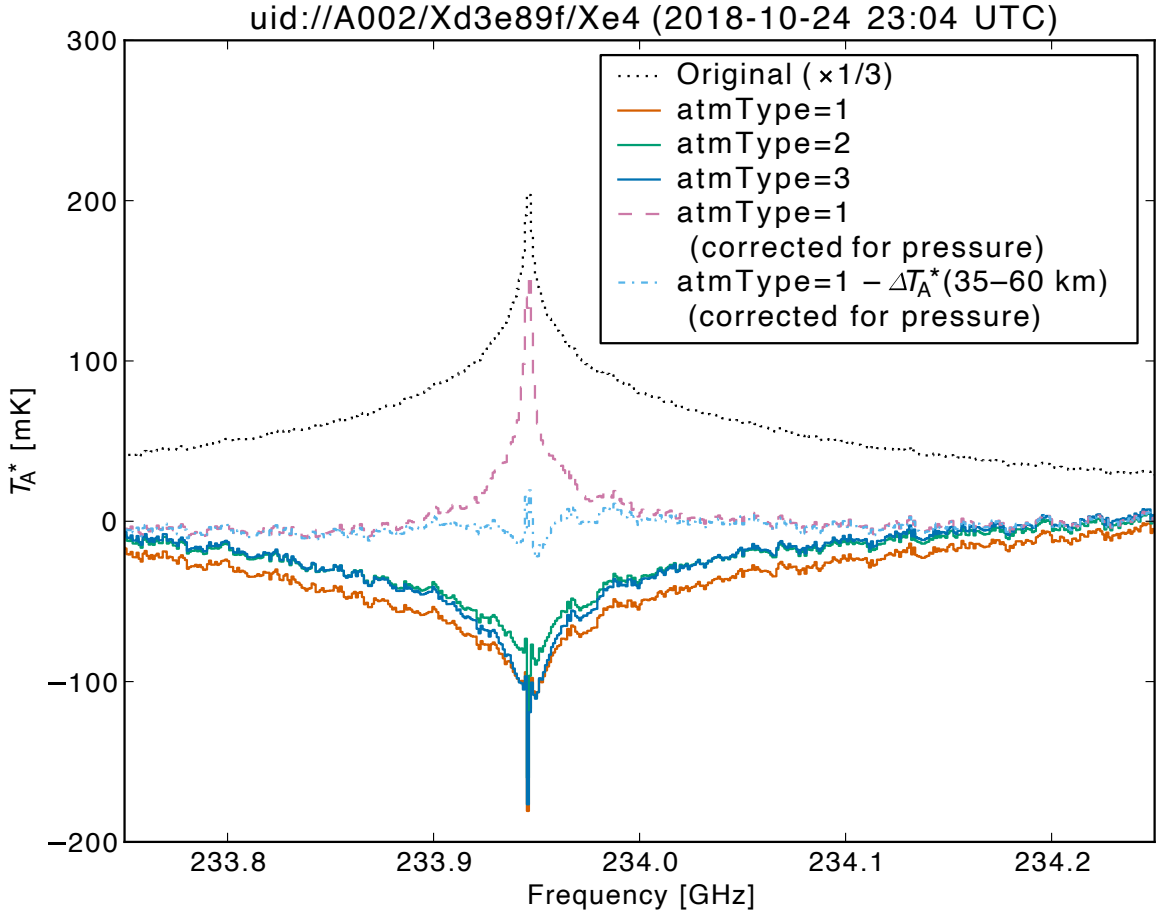


Figure 11. The uncorrected and corrected average T_A^* spectra of the 233.95 GHz $^{16}\text{O}^{18}\text{O}$ line from the EB uid://A002/Xd3e89f/Xe4 (SB 24013+04_a.06_TP, project 2018.1.00443.S). The uncorrected spectrum (dotted line) is divided by 3. The corrected spectra using `atmType` = 1, 2, and 3 are shown as solid lines. For `atmType` = 1, the spectrum corrected for the pressure is shown as a dashed line, and another spectrum from which the pressure-corrected ΔT_A^* for 35–60 km altitude is further subtracted is displayed as a dash-dotted line (see the text). Note that the small wiggles seen in the line wings are unrelated to the correction.

We described a method to mitigate the atmospheric artifacts in single-dish radio spectra using the ATM model and presented the results for the data taken with the ALMA TP Array. The residual atmospheric line intensities were suppressed typically by an order of magnitude, dependent upon the species and transitions. The best-fitting value of one of the ATM model parameters, `atmType`, was demonstrated to be dependent on the observing seasons for the 231.28 GHz O_3 line. A further study of parameter optimization for other lines may help better mitigate the residual lines in future data processing. We also compared the ATM model with MERRA-2 meteorological reanalysis datasets for two transitions; the 231.28 GHz O_3 and 233.95 GHz $^{16}\text{O}^{18}\text{O}$ lines. This comparison suggests that the extraction of these two transitions from total power spectra is improved if the difference between the ATM and MERRA-2 models is taken into account. The method described in this article will be implemented as a task in CASA version 6.2. It will also be included in the pipeline data processing for the ALMA TP Array in the future. The expectation is that the use of the algorithm described in this article will reduce the number of observations that cause difficulties in the Quality Assurance Level 2 (cf. Remijan et al. 2020) due to atmospheric artifacts.

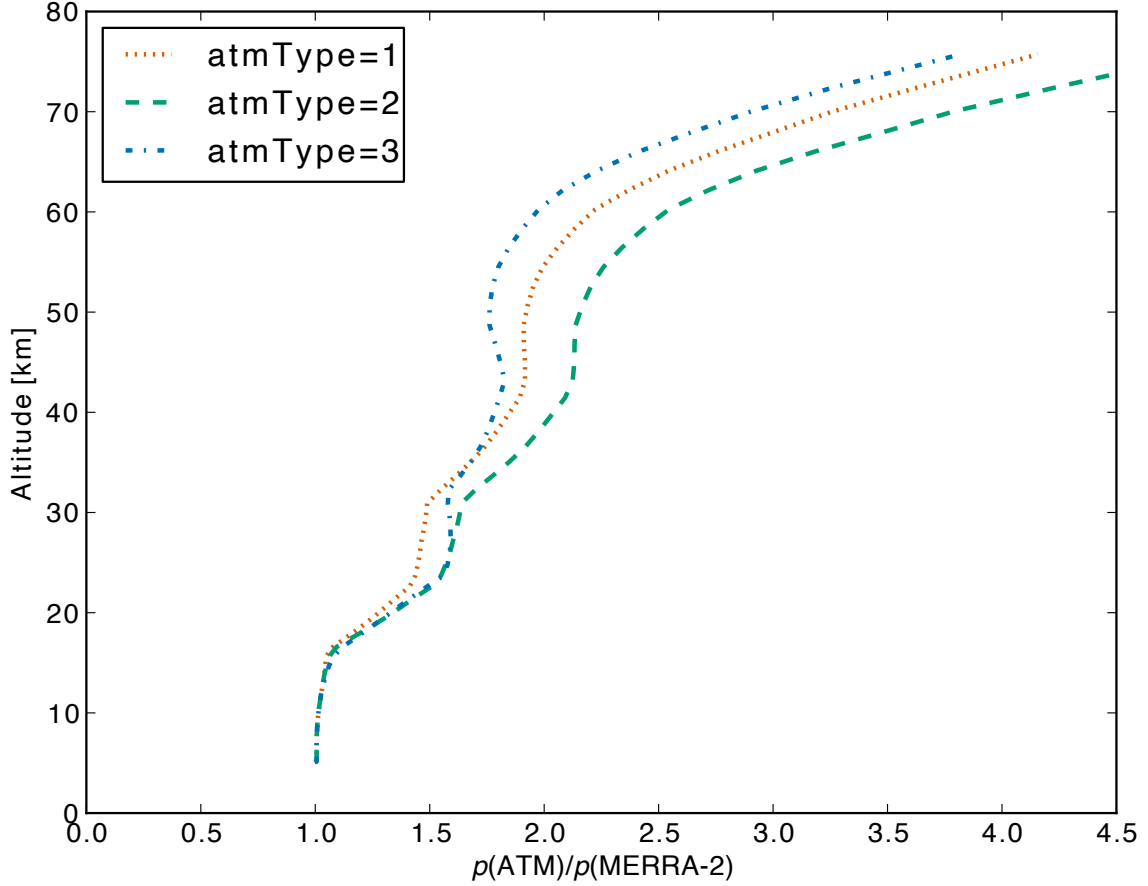


Figure 12. The ratio between the vertical pressure profiles from ATM and MERRA-2 for uid://A002/Xd3e89f/Xe4. The MERRA-2 three-hourly instantaneous dataset (Global Modeling and Assimilation Office (GMAO) 2015a) at (67°5 W, 23°0 S), 2018-10-25 00:00 UTC is used.

ACKNOWLEDGMENTS

This article makes use of the following ALMA data: ADS/JAO.ALMA#2015.1.00121.S, ADS/JAO.ALMA#2015.1.00274.S, ADS/JAO.ALMA#2015.1.00357.S, ADS/JAO.ALMA#2015.1.00667.S, ADS/JAO.ALMA#2015.1.00717.S, ADS/JAO.ALMA#2015.1.00908.S, ADS/JAO.ALMA#2015.1.01539.S, ADS/JAO.ALMA#2016.1.00203.S, ADS/JAO.ALMA#2016.1.00386.S, ADS/JAO.ALMA#2016.1.01346.S, ADS/JAO.ALMA#2016.1.01541.S, ADS/JAO.ALMA#2017.1.00093.S, ADS/JAO.ALMA#2017.1.00716.S, ADS/JAO.ALMA#2018.1.00272.S, ADS/JAO.ALMA#2018.1.00443.S, and ADS/JAO.ALMA#2018.1.00770.S. ALMA is a partnership of ESO (representing its member states), NSF (USA) and NINS (Japan), together with NRC (Canada), MOST and ASIAA (Taiwan), and KASI (Republic of Korea), in cooperation with the Republic of Chile. The Joint ALMA Observatory is operated by ESO, AUI/NRAO and NAOJ. This article makes use of the MERRA-2 datasets *inst3_3d_asm_Nv* and *inst3_3d_chm_Nv* retrieved on 2020 Dec 9 via Goddard Earth Sciences Data and Information Services Center. We thank the anonymous referee for valuable comments and suggestions. T.S. was supported by the ALMA Japan Research Grant of NAOJ ALMA Project, NAOJ-ALMA-248.

Facilities: ALMA

Software: CASA (McMullin et al. 2007)

REFERENCES

- Gelaro, R., McCarty, W., Suárez, M. J., et al. 2017, *Journal of Climate*, 30, 5419
- Global Modeling and Assimilation Office (GMAO). 2015a, MERRA-2 inst3_3d_asm_Nv: 3d, 3-Hourly, Instantaneous, Model-Level, Assimilation, Assimilated Meteorological Fields V5.12.4, Greenbelt, MD, USA, Goddard Earth Sciences Data and Information Services Center (GES DISC), doi:10.5067/WWQSQ8IVFW8
- . 2015b, MERRA-2 inst3_3d_chm_Nv: 3d, 3-Hourly, Instantaneous, Model-Level, Assimilation, Carbon Monoxide and Ozone Mixing Ratio V5.12.4, Greenbelt, MD, USA, Goddard Earth Sciences Data and Information Services Center (GES DISC), doi:10.5067/HO9OVZWF3KW2
- Iguchi, S., Morita, K.-I., Sugimoto, M., et al. 2009, *PASJ*, 61, 1
- Kutner, M. L., & Ulich, B. L. 1981, *ApJ*, 250, 341
- Liebe, H. J. 1989, *International Journal of Infrared and Millimeter Waves*, 10, 631
- Mangum, J. G., Emerson, D. T., & Greisen, E. W. 2007, *A&A*, 474, 679
- McMullin, J. P., Waters, B., Schiebel, D., Young, W., & Golap, K. 2007, *Astronomical Society of the Pacific Conference Series*, Vol. 376, *CASA Architecture and Applications*, ed. R. A. Shaw, F. Hill, & D. J. Bell, 127
- Nikolic, B., Bolton, R. C., Graves, S. F., Hills, R. E., & Richer, J. S. 2013, *A&A*, 552, A104
- Pardo, J., Pagani, L., Gerin, M., & Prigent, C. 1995, *JQSRT*, 54, 931
- Pardo, J. R., Cernicharo, J., & Pagani, L. 1998, *J. Geophys. Res.*, 103, 6189
- Pardo, J. R., Cernicharo, J., & Serabyn, E. 2001, *IEEE Transactions on Antennas and Propagation*, 49, 1683
- Remijan, A., Biggs, A., Cortes, P., et al. 2020, *ALMA Technical Handbook*, ALMA Doc. 8.3, ver. 1.0, <https://almascience.nrao.edu/documents-and-tools/cycle8/alma-technical-handbook>
- Sawada, T., Ikeda, N., Sunada, K., et al. 2008, *PASJ*, 60, 445
- Stirling, A., Hills, R., Richer, J., & Pardo, J. 2004, 183 GHz water vapour radiometers for ALMA: Estimation of phase errors under varying atmospheric conditions, <https://library.nrao.edu/public/memos/alma/main/memo496.pdf>, The ALMA Project, ALMA Memo Series 496
- Ulich, B. L., & Haas, R. W. 1976, *ApJS*, 30, 247
- Vaughan, G. 1982, *Nature*, 296, 133